

Generalizing Deepfake Video Detection with Plug-and-Play: Video-Level Blending and Spatiotemporal Adapter Tuning

Zhiyuan Yan^{1,2}, Yandan Zhao², Shen Chen², Xinghe Fu², Taiping Yao²,
Shouhong Ding², Li Yuan¹

¹Peking University

²Tencent YouTu Lab

Abstract

Three key challenges hinder the development of current deepfake video detection: (1) Temporal features can be complex and diverse: how can we identify general temporal artifacts to enhance model generalization? (2) Spatiotemporal models often lean heavily on one type of artifact and ignore the other: how can we ensure balanced learning from both? (3) Videos are naturally resource-intensive: how can we tackle efficiency without compromising accuracy?

This paper attempts to tackle the three challenges jointly. **First**, inspired by the notable generality of using image-level blending data for image forgery detection, we investigate whether and how video-level blending can be effective in video. We then perform a thorough analysis and identify a previously underexplored temporal forgery artifact: Facial Feature Drift (FFD), which commonly exists across different forgeries. To reproduce FFD, we then propose a novel **Video-level Blending data (VB)**, where VB is implemented by blending the original image and its warped version frame-by-frame, serving as a hard negative sample to mine more general artifacts. **Second**, we carefully design a lightweight Spatiotemporal Adapter (**StA**) to equip a pretrained image model (both ViTs and CNNs) with the ability to capture both spatial and temporal features jointly and efficiently. StA is designed with two-stream 3D-Conv with varying kernel sizes, allowing it to process spatial and temporal features separately. Extensive experiments validate the effectiveness of the proposed methods; and show our approach can generalize well to previously unseen forgery videos, even the just-released (in 2024) SoTAs. We release our code and pretrained weights at <https://github.com/YZY-stack/StA4Deepfake>.

1 Introduction

Current deepfake¹ technology enables effortless manipulation of facial identities in video content, bringing many impressive applications in fields such as movie-making and entertainment. However, this technology can also be misused for malicious purposes, including violating personal privacy, spreading misinformation, and eroding trust in digital media. Hence, there is a pressing need to establish a reliable system for detecting deepfake videos.

¹The term “deepfake” hereafter mainly refers to **face** forgery, typically referring to face-swapping. The entire (or natural) image synthesis is not within our scope.

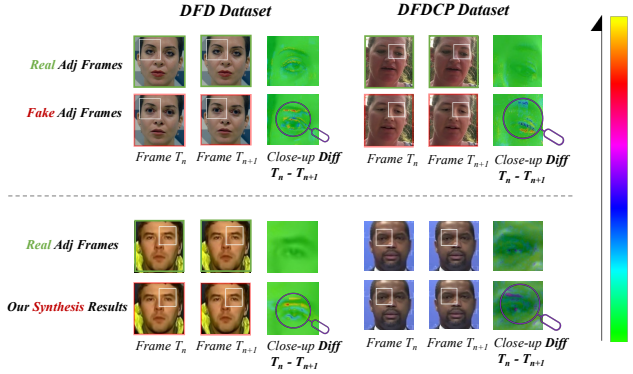


Figure 1: Illustration of Facial Feature Drift (FFD) phenomena. We empirically select two relatively static consecutive frames to demonstrate the facial temporal inconsistency between fake frames (FFD), even when the two frames appear similar at the image level. More demonstrations can be seen in the supplementary.

Most prior deepfake detectors (Zhou et al. 2017; Li and Lyu 2018; Rossler et al. 2019; Yang, Li, and Lyu 2019) perform well within the same dataset. However, they often fail to generalize well in cross-dataset scenarios where training and testing data distributions differ. Training with synthetic (blending) images appears to be one of the most effective solutions to this problem, which encourages detectors to learn generic representations (*e.g.*, blending boundaries and inconsistencies between inner and outer faces) for deepfake detection (Li et al. 2020a; Shiohara and Yamasaki 2022). Given the notable success of image-level blending, we ask: *what about video-level blending? Can this method also be applied to learn general forgery artifacts in the video domain?* (**Research-Question-1**).

To this end, we perform a comprehensive examination of current realistic forgery videos and discover an inconsistency in the facial organs between forgery frames (as illustrated in Fig. 1). We term this phenomenon as the *Facial Feature Drift (FFD)*. As illustrated in Fig. 1, even when two consecutive frames appear relatively static (possibly without other unrelated effects), subtle unnatural drift and flickering can be observed within facial features (*e.g.*, eyes, nose, *etc.*).

This observation provides reasonable evidence that unnatural forgery artifacts are indeed present in the temporal domain of manipulated videos.

Intuitively, the root cause of FFD can be attributed to the frame-by-frame face-swapping operation employed by existing deepfake algorithms. To understand the underlying reasons, we argue that the primary factor is the randomness during the generation process of fake faces. Deepfake algorithms typically create a fake frame by using DNNs to generate a counterfeit inner face. Subsequently, they perform a blending operation to integrate this generated face back into the original background. Given this context, it is important to note that the inner face between different frames within a single generated video may exhibit variations, as the DNN is not a deterministic function. Consequently, this leads to inconsistencies in the generation process of fake faces.

To effectively make the detection model capture FFD in the given deepfake, we introduce a novel **Video-level Blending** data called **VB** to reproduce FFD. The overall creation pipeline of VB is illustrated in Fig. 2. Specifically, we generate VB by first applying warping operations separately to facial organs and then performing image-level self-blending to generate one synthesis image. The process is repeatedly conducted for all frames within one clip to create a set of synthesis images (video-level pseudo-fakes). VB can serve as the hard negative samples for mining more general discriminative features for detection. But why do we specifically focus on facial features? This is mainly because regions, such as skin, are low-level areas that can be sensitive to random perturbations (*e.g.*, compression), while facial features typically possess a more robust high-level layout. Also, we can observe more obvious temporal inconsistency within the facial organs in Fig. 1.

Additionally, as suggested by (Zheng et al. 2021; Wang et al. 2023), naively training a temporal detector may result in the model only focusing on easier types of artifacts and overlooking more challenging ones (*e.g.*, learning spatial only). *So how do we jointly learn temporal and spatial features without heavily relying on one?* (**Research-Question-2**). Also, *as videos are naturally more complex than images with multiple frames to be computed, how do we address the efficiency issue?* (**Research-Question-3**). Instead of designing a new video architecture from scratch, we propose an alternative approach: to “convert” a pretrained image model into a video model, enabling the model to learn additional temporal information. Specifically, we meticulously design a lightweight, plug-and-play Spatiotemporal Adapter (StA) that equips an image model (*e.g.*, ViT or CNN) with spatiotemporal reasoning capabilities. Throughout the whole training process, only the added adapters are updated, which significantly reduces the training cost and allows us to leverage the powerful generalization capabilities of SoTA image models (*e.g.*, CLIP).

Overall, this work addresses three key challenges in detecting deepfake videos (mentioned in **Research Questions**). Our main contributions are two-fold as follows.

- We discover a novel and previously underexplored forgery artifact in the temporal domain. After careful

examination of current forgery videos, we observe that there exists a subtle inconsistent artifact in the location and shape of facial organs between frames. We term it **Facial Feature Drift** (FFD), which is potentially produced within the process of frame-by-frame face-swapping operation. To simulate this, we propose a **Video-level Blending** (VB) to aid the model in learning general temporal forgery features.

- We propose a plug-and-play adapter for learning both spatial and temporal forgery artifacts. By solely training the adapters for fine-tuning, we are allowed to leverage the powerful generalization ability of SoTA image models (*e.g.*, CLIP).

2 Related Work

2.1 Deepfake Image Detection

Conventional image detectors (Nguyen, Yamagishi, and Echizen 2019; Rossler et al. 2019) typically focus on developing optimal CNN architectures (*e.g.*, MesoNet, CapsuleNet). However, these methods often overlook the details present in the frequency domain of fake images, such as compression artifacts. To this end, several works (Qian et al. 2020; Gu et al. 2022a) utilize frequency information to improve the performance of detectors. Other notable directions are focusing on some specific representations, *i.e.*, 3D decomposition (Zhu et al. 2021), disentanglement (Liang, Shi, and Deng 2022; Yan et al. 2023b), erasing technology (Wang and Deng 2021), theoretic information (Sun et al. 2022a), debiased learning (Cheng et al. 2024), facial landmark (Yan et al. 2022), and parameter-efficient tuning (Kong, Li, and Wang 2023; Kong et al. 2024b,a). Recently, several works (Jia et al. 2024; Shi et al. 2024) attempt to detect deepfakes with training-free pipelines. These works mostly utilize designed algorithms for detection from the view of representation learning. Another important direction of image forgery detection is data synthesis (image blending). We will discuss it separately in another subsection.

2.2 Deepfake Video Detection

There are parts of works (Zhou et al. 2017) that focus on temporal artifacts. An early work (Haliassos et al. 2021) (in 2021) proposes to leverage the temporal inconsistency of the mouth movement. This work utilizes a pre-trained model to learn the natural lip movement as prior on a lip-reading dataset. FTCN (Zheng et al. 2021) explores directly training a fully temporal 3D ConvNets with an attached temporal Transformer. However, detecting without spatial information may harm the generalization capability. STIL (Gu et al. 2021) considers both spatial and temporal inconsistency and designs a spatiotemporal inconsistency Learning framework for deepfake video detection. RealForensics (Haliasos et al. 2022) introduces audio information and leverages self-supervised learning for representation learning. Very recently, wang *et al.* (Wang et al. 2023) propose a new learning method that alternatively trains and freezes the spatial and temporal convolutional layers in a 3D CNN (*e.g.*, I3D R50).

The result shows the importance of leveraging both spatial and temporal features for detecting deepfakes.

2.3 Deepfake Detectors Based on Data Synthesis

Image-level Data Synthesis. One effective approach in deepfake detection is to use synthetic data (or blending data/images) for training. This strategy encourages models to learn generic representations for detecting deepfakes, such as blending boundaries and inconsistency between the inner and outer faces (Shiohara and Yamasaki 2022). For instance, in the early stages, FWA (Li and Lyu 2018) employs a self-blending strategy by applying image transformations (*e.g.*, down-sampling) to the facial region and then warping it back into the original image. This process is designed to learn the wrapping artifacts during the deepfake generation process. Another noteworthy contribution is Face X-ray (Li et al. 2020a), which explicitly encourages detectors to learn the blending boundaries of fake images. Furthermore, SLADD (Chen et al. 2022) introduces an adversarial method to dynamically generate the most challenging blending choices for synthesizing data. Rather than swapping faces between two different identities, a recent art, SBI (Shiohara and Yamasaki 2022), proposes to swap with the same person’s identity to reach a high-realistic face-swapping. Given the notable generalization performance for detecting image forgery by using synthetic data, it remains an open question whether and how video-level synthetic data can be effective.

Video-level Data Synthesis. Compared to image-level data synthesis (blending), very little works pay attention to designing a suitable video-level blending method. To the best of our knowledge, we identify one notable work (Wang et al. 2023) that attempts to design video-level data synthesis by using techniques such as dropping/repeating one frame within one clip. However, it is possible that these common operations might not explicitly represent the general forgery pattern. Recall that in the image domain, we use blending technology to synthesize the forgery artifact since the blending artifact commonly exists across different forgeries, generally. So there are two main challenges: (1) What kinds of features generally exist in the temporal domain? (2) How to use blending to simulate it like the image data synthesis? We will show our video-level method in the following section.

3 Method

3.1 Notation

We first introduce some important notations and the detailed summary can be found in supplementary. Suppose we have a frame \mathbf{I} from the original video. We definite that the facial region R contains several specific facial regions r such as eyes, eyebrows, nose, and mouth. Let \mathbf{L}_z be the landmark of region z , where z can be a specific facial region r or the whole facial region R . To transform landmarks, where transformation parameters are sampled from the uniform distribution, we set 3 hyperparameters u_r, u_s, u_t to be the maximum rotation angle, scaling factor, and translation distance, respectively. After landmark perturbation, we will derive a

new landmark \mathbf{L}_R^* of the facial region R and the corresponding warped image \mathbf{I}_{warp} . We consider the mask $\mathbf{M}_r(x, y)$ for region r , indicating the blending weight at pixel (x, y) . At last, we obtain the final blended frame \mathbf{I}' which is composed of \mathbf{I}'_r : blended frame about region r , and α_r is used to control the blending weight for region r . To better illustrate our method, we denote $\text{dist}(x, y, \mathbf{L}_r)$ as a signed distance function calculating the shortest distance from a pixel (x, y) to the closest landmark in \mathbf{L}_r , fdist_r as a predefined fall-off distance for the mask of region r and $\text{clip}(x, \text{min}, \text{max})$ as a function that limits x within the range $[\text{min}, \text{max}]$.

3.2 Video-level Data Synthesis

Although contemporary deepfake generation algorithms are adept at producing realistic forgeries on a frame-by-frame basis, they frequently overlook the consistency between frames. This oversight results in temporal artifacts like flickering and discontinuity. A common temporal artifact known as Facial Feature Drift (FFD) arises from the frame-by-frame process of face-swapping algorithms. This artifact is characterized by inconsistencies in the placement and contours of facial features from one frame to the next. To exploit the generalization potential of FFD for video-level deepfake detection, we introduce a novel synthetic training data, VB: simulating the Facial Feature Drift phenomenon through landmark perturbation and region mask extraction on facial organs across video frames. The self-image blending process involves several steps, including warped image generation, region mask extraction, dynamic blending, and composite image formation, each contributing to the final blended video frame. Note that perturbation parameters u_r, u_s , and u_t introduce variability in the appearance of facial regions across frames, contributing to the realism of the video by mimicking natural movements and expressions.

Landmark perturbation. Our goal is to manifest FFD, that is perturbation of landmarks region. Assuming that the perturbation parameter follows the uniform distribution $U_{[0, u_i]}, i \in \{r, s, t\}$, we sample parameters for current images perturbation. And we can derive transformed landmarks $\mathbf{L}_R^* = \mathbf{A}\mathbf{L}_R$, where \mathbf{A} is the affine transformation matrix corresponding to sampled parameters. As a result, warp transformation can be written as: $\mathbf{I}_{\text{warp}} = \mathbf{A}\mathbf{I}$.

Region Mask Extraction. Our method focuses on facial regions, and thus requires a mask to keep other regions the same while changing regions of interest. At the same time, we hope that the closer to the landmark, the more obvious the traces of perturbation will be. For each facial region r with landmarks \mathbf{L}_r , the generation of the mask \mathbf{M}_r is formulated as:

$$\mathbf{M}_r(x, y) = 1 - \text{clip}\left(\frac{\text{dist}(x, y, \mathbf{L}_r)}{\text{fdist}_r}, 0, 1\right), r \in R. \quad (1)$$

This equation ensures that the mask \mathbf{M}_r smoothly transitions from 1 (fully included in blending) to 0 (excluded from blending) as the distance from the landmarks increases, up to a maximum defined by fdist_r . The hyper-parameter fdist_r defines the farthest range that will be included in blending.

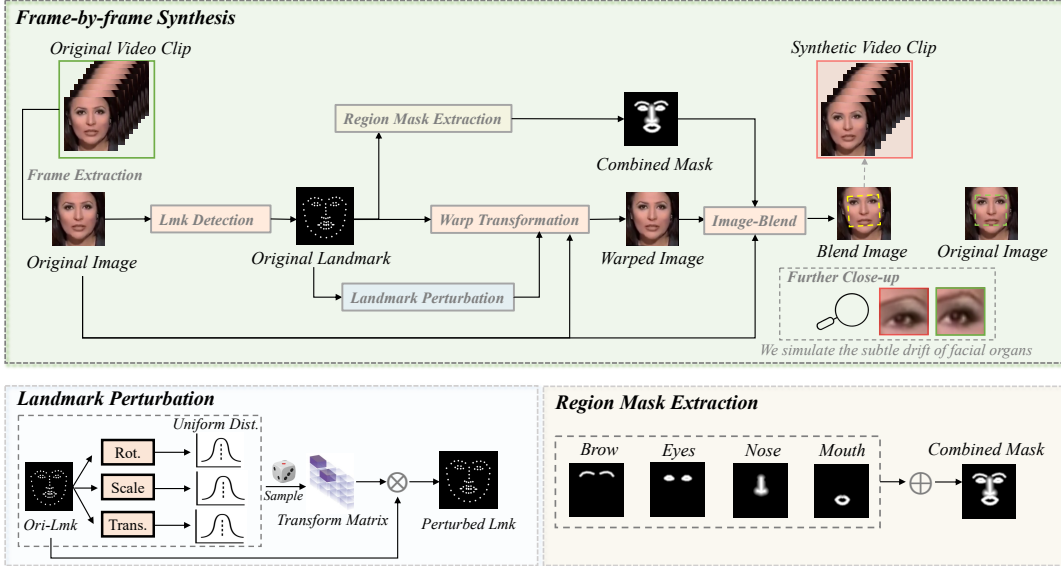


Figure 2: The overall pipeline of the proposed video-level blending method (VB). The whole process involves repeatedly performing **Frame-by-Frame Synthesis** for a video clip. Two main steps in the frame-by-frame synthesis are **Landmark Perturbation** and **Region Mask Extraction**, where the former is designed to add random perturbation to the given facial landmarks and the latter is to extract the mask of each facial organ. The detailed algorithms can be seen in the text.

Algorithm 1: Algorithm of VB

Input: Face image \mathbf{I} ; Landmarks \mathbf{L}_R ; Fall-off distance $\text{fdist}_r, r \in R$; Upper bound of perturbation parameters $u_i, i \in \{r, s, t\}$

Output: Blended image \mathbf{I}'

- 1: \triangleright Step 1: **Warp transformation**
- 2: Perturbation parameters $\sim U_{[0, u_i]}$
- 3: Derive affine matrix \mathbf{A}
- 4: $\mathbf{I}_{\text{warp}} \leftarrow \mathbf{A}\mathbf{I}$
- 5: **for** r in R **do**
- 6: \triangleright Step 2: **Mask Generation**
- 7: $\mathbf{M}_r \leftarrow 1 - \text{clip}\left(\frac{\text{dist}(\mathbf{I}, \mathbf{L}_r)}{\text{fdist}_r}\right)$
- 8: \triangleright Step 3: **Dynamic Blending**
- 9: $\mathbf{I}'_r \leftarrow (\mathbf{M}_r \cdot \mathbf{I}_{\text{warp}}) + ((1 - \mathbf{M}_r) \cdot \mathbf{I})$
- 10: **end for**
- 11: \triangleright Step 4: **Composite Images**
- 12: $\mathbf{I}' \leftarrow \sum_{r \in R} \alpha_r \cdot \mathbf{I}'_r$
- 13: **return** \mathbf{I}'

Dynamic Blending. As we set various masks for different regions, we first create a blended image for each special region. Specifically, the dynamic blending process for a region r is described by the equation:

$$\mathbf{I}'_r = (\mathbf{M}_r \cdot \mathbf{I}_{\text{warp}}) + ((1 - \mathbf{M}_r) \cdot \mathbf{I}), r \in R. \quad (2)$$

Here, \mathbf{I}_{warp} is derived from \mathbf{I} by applying an affine transformation that introduces perturbations in rotation, scale, and translation, simulating natural movements. \mathbf{M}_r dictates how much of \mathbf{I}_{warp} versus \mathbf{I} is used at each pixel, achieving a blended effect in the region r .

Composite Image Formation. Finally, VB image \mathbf{I}' can be obtained through compositing blended images of different facial regions. The composite process is formulated as:

$$\mathbf{I}' = \sum_{r \in R} \alpha_r \cdot \mathbf{I}'_r, \quad \text{where } \sum_{r \in R} \alpha_r = 1. \quad (3)$$

Each region r contributes to \mathbf{I}' based on its blending weight α_r , allowing for the balanced integration of all facial features into the cohesive final image. After generating a VB frame corresponding to each frame of the video, we synthesize VB frames into a new VB video.

3.3 Spatiotemporal Adapters (StA)

A video can be naturally represented as a stack of image frames. One challenging problem is to capture both spatial and temporal forgery artifacts without heavily relying on one type of artifact. Previous works generally follow two mainstream frameworks: (1) Utilizing 3D CNN (e.g., I3D R50) for capturing spatiotemporal information from forgery videos (Zheng et al. 2021; Wang et al. 2023); (2) Utilizing two-stream architecture to learn the spatial and temporal features in two separate branches (Masi et al. 2020; Zhou et al. 2017). These two paradigms typically involve fully fine-tuning for both spatial and temporal modules. However, training all layers of both spatial and temporal modules will inevitably introduce a large number of learnable parameters, making the optimization and training procedure challenging. On the other hand, the image model (especially ViT-based image SoTA) is developing rapidly. It is well-known that these image SoTAs have achieved notable performance in several downstream computer vision tasks (e.g., multimodality (Ganz et al. 2024)). Therefore, *can we leverage the power of these SoTA image models to effectively and efficiently finetune the face forgery detection task?* The key

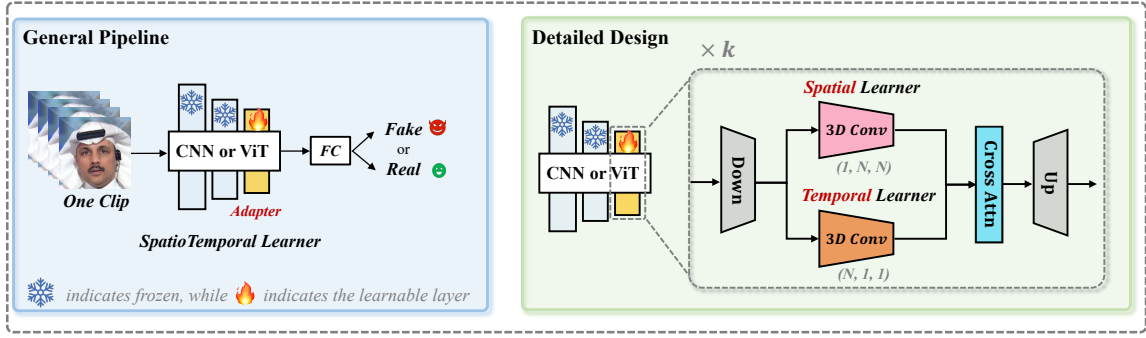


Figure 3: The overall pipeline of the proposed adapter-based strategy. We propose a novel and efficient adapter-based method that can be plug-and-play inserted into any SoTA image detector.

challenge is to perform the temporal forgery feature modeling in a given image model.

To this end, we proposed a lightweight adapter for spatiotemporal feature finetuning. Our proposed framework is simple but efficient and effective (shown in Fig. 3). Differing from previous frameworks for full-parameters fine-tuning, in our framework, only the lightweight adapter is learnable during the training process. The adapter contains two 3D-Conv layers for spatial and temporal modeling, followed by a cross-attention layer to extract the high-level relationship between them. The 3D-Conv for spatial modeling is with the kernel size of $(1, N, N)$, capturing the spatial-only information, while the 3D-Conv for temporal is $(N, 1, 1)$, for temporal-only modeling.

Formally, given a video clip $\mathbf{x}_k^{in} \in \mathbb{R}^{T \times H \times W \times C}$ (T frames within the same video), obtained from the l -th stage of the pretrained image backbone. Where C is the channels of feature maps, $H \times W$ for the spatial size, and T represents the number of frames within the video clip. The spatial and temporal features can be computed as follows:

$$\begin{aligned} \mathbf{e}_k^s &= \text{3DConv}_s (\mathbf{W}_{\text{down}} \cdot \mathbf{x}_k^{in}), \\ \mathbf{e}_k^t &= \text{3DConv}_t (\mathbf{W}_{\text{down}} \cdot \mathbf{x}_k^{in}), \end{aligned} \quad (4)$$

where $\mathbf{W}_{\text{down}} \in \mathbb{R}^{C \times C'}$. 3DConv_s and 3DConv_t represent the 3D-Conv layers for spatial and temporal modeling. Specifically, we implement three DepthWise 3D-Conv layers with different scales (*i.e.*, 3, 5, 7) to capture multi-scale features. After obtaining both the spatial (\mathbf{e}_k^s) and temporal feature maps (\mathbf{e}_k^t), we apply a cross-attention layer to capture the high-level relationship between spatial and temporal features. First, we flatten the spatial and temporal dimensions and then permute the dimensions to prepare the tensors for multi-head attention: $\mathbf{e}_k^s \rightarrow \mathbf{p}_k^s \in \mathbb{R}^{(T \times H \times W) \times C}$ and $\mathbf{e}_k^t \rightarrow \mathbf{p}_k^t \in \mathbb{R}^{(T \times H \times W) \times C}$. We then apply cross-attention between permuted spatial and temporal features:

$$\begin{aligned} \mathbf{S2T} &= \text{MultiHeadAttention}(\mathbf{p}_k^t, \mathbf{p}_k^s, \mathbf{p}_k^s), \\ \mathbf{T2S} &= \text{MultiHeadAttention}(\mathbf{p}_k^s, \mathbf{p}_k^t, \mathbf{p}_k^t), \end{aligned} \quad (5)$$

where $\mathbf{S2T}$ represents the result of integrating spatial information into the temporal dimension, while $\mathbf{T2S}$ represents

the result of integrating temporal information into the spatial dimension.

The attention outputs are reshaped back to their original dimensions: $\mathbf{S2T}^{\text{perm}} \rightarrow \mathbf{S2T}^{\text{orig}} \in \mathbb{R}^{B \times C \times T \times H \times W}$ and $\mathbf{T2S}^{\text{perm}} \rightarrow \mathbf{T2S}^{\text{orig}} \in \mathbb{R}^{B \times C \times T \times H \times W}$. The final output is obtained by averaging the two attention results and adjusting the channels by an Upsampling layer (*up*):

$$\mathbf{x}_k^{\text{out}} = \frac{1}{2} (\mathbf{S2T}^{\text{orig}} + \mathbf{T2S}^{\text{orig}}) \cdot \mathbf{W}_{\text{up}}. \quad (6)$$

In the whole training process, only the added modules are updated (*i.e.*, adapters and cross-attention layers, *etc*), significantly reducing the training cost.

4 Results

4.1 Setup

Dataset. To evaluate the generalization ability of our proposed framework, we conduct experiments on **eight** commonly used datasets: FaceForensics++ (FF++) (Rossler et al. 2019), Deepfake Detection Challenge (DFDC) (Dolhansky et al. 2020), the preview version of DFDC (DFDCP) (Dolhansky et al. 2019), DeepfakeDetection (DFD) (Deepfakedetection. 2021), Celeb-DF-v2 (CDF-v2) (Li et al. 2020b), DeeperForensics (DFo) (Jiang et al. 2020), Wild-Deepfake (WDF) (Zi et al. 2020), and FFIW (Zhou et al. 2021). We also evaluate the models on the **just-released** (in 2024) deepfake dataset DF40 (Yan et al. 2024), which contains 40 distinct forgery methods. We select **eight face-swapping methods** generated from the FF++ domain for our evaluation. In line with the standard deepfake benchmark (Yan et al. 2023c), we utilize the c23 version of FF++ for training and other datasets for testing.

Implementation Details. We utilize ViT-114 (Dosovitskiy et al. 2020) as the backbone for extracting forgery features. By default, the model parameters are initialized through pre-training on CLIP (Radford et al. 2021). We also investigate other architectures in Tab. 4. In our experiments, we uniformly sample 32 frames from each video during training and randomly select 8 consecutive frames as a clip for each iteration. All preprocessing and training codebases are aligned to the deepfake benchmark (Yan et al. 2023c) for a

Table 1: **Protocol-1:** Cross-dataset evaluations with **image detectors**. All detectors are trained on FF++_c23 (Rossler et al. 2019) and evaluated on other datasets. The best results are highlighted in bold and the second is underlined. * indicates the results are directly cited from their original papers, otherwise the results are reproduced in our benchmark.

Detector	Venues	CDF-v2	DFD	DFDC	DFDCP	DFo	WDF	FFIW	Avg.
F3Net (Qian et al. 2020)	ECCV 2020	0.789	0.844	0.718	0.749	0.730	0.728	0.649	0.743
SPSL (Liu et al. 2021)	CVPR 2021	<u>0.799</u>	0.871	0.724	0.770	0.723	0.702	0.794	0.769
SRM (Luo et al. 2021)	CVPR 2021	0.840	0.885	<u>0.695</u>	0.728	0.722	0.702	0.794	0.767
CORE (Ni et al. 2022)	CVPRW 2022	0.809	0.882	0.721	0.720	0.765	0.724	0.710	0.762
RECCE (Cao et al. 2022)	CVPR 2022	0.823	0.891	0.696	0.734	0.784	0.756	0.711	0.779
DCL (Sun et al. 2022b)	AAAI 2022	0.882	0.921	<u>0.750</u>	0.769	0.975	0.776	0.863	0.851
SLADD* (Chen et al. 2022)	CVPR 2022	0.797	-	<u>0.772</u>	-	-	-	-	-
SBI (Shiohara and Yamasaki 2022)	CVPR 2022	0.886	0.827	0.717	0.848	0.899	0.703	0.866	0.821
UIA-VIT* (Zhuang et al. 2022)	ECCV 2022	0.889	-	-	0.795	-	-	-	-
UCF (Yan et al. 2023b)	ICCV 2023	0.837	0.867	0.742	0.770	0.808	0.774	0.697	0.785
SeeABLE* (Yan et al. 2023b)	ICCV 2023	0.873	-	<u>0.759</u>	0.863	-	-	-	-
IID* (Huang et al. 2023)	CVPR 2023	0.838	0.939	-	<u>0.812</u>	-	-	-	-
CFM (Luo et al. 2023)	TIFS 2023	0.897	0.952	0.706	0.802	<u>0.976</u>	<u>0.823</u>	0.831	<u>0.856</u>
LSDA (Yan et al. 2023a)	CVPR 2024	<u>0.898</u>	0.956	0.735	<u>0.812</u>	0.892	0.756	0.879	0.847
Ours	-	0.947	0.965	0.843	0.909	0.991	0.848	0.921	0.911
		($\uparrow 4.9\%$)	($\uparrow 0.9\%$)	($\uparrow 9.3\%$)	($\uparrow 6.1\%$)	($\uparrow 1.5\%$)	($\uparrow 2.5\%$)	($\uparrow 4.2\%$)	($\uparrow 5.5\%$)

Table 2: **Protocol-2:** Cross-manipulation evaluations **within FF++ domain**. We use the just-released latest deepfake dataset DF40 (Yan et al. 2024) and select eight typical face-swapping methods generated **on the FF++ domain**, allowing us to perform the cross-manipulation evaluation (domain unchanged).

Detector	UniFace	BlendFace	MobileSwap	e4s	FaceDancer	FSGAN	Inswap	SimSwap	Avg.
RECCE (Cao et al. 2022)	0.898	0.832	0.925	0.683	0.848	0.949	0.848	0.768	0.844
SBI (Shiohara and Yamasaki 2022)	0.724	0.891	0.952	<u>0.750</u>	0.594	0.803	0.712	0.701	0.766
UCF (Yan et al. 2023b)	0.831	0.827	<u>0.950</u>	0.731	<u>0.862</u>	0.937	0.809	0.647	0.824
AltFreezing (Wang et al. 2023)	0.947	0.951	0.851	0.605	0.836	<u>0.958</u>	<u>0.927</u>	0.797	0.859
Ours	0.960	<u>0.906</u>	0.946	0.980	0.912	0.964	0.937	0.931	0.942

Table 3: **Protocol-3:** Cross-dataset evaluations with **video detectors**. The results of these detectors are directly cited from their original papers.

Detector	Venues	CDF-v2	DFDC	Avg.
LipForensics (Haliassos et al. 2021)	CVPR 2021	0.824	0.735	0.780
FTCN (Zheng et al. 2021)	ICCV 2021	0.869	0.740	0.805
HCIL (Gu et al. 2022b)	ECCV 2022	0.790	0.692	0.741
RealForensics (Haliassos et al. 2022)	CVPR 2022	0.857	0.759	0.808
LTTD (Guan et al. 2022)	NeurIPS 2022	0.893	<u>0.804</u>	<u>0.849</u>
AltFreezing (Wang et al. 2023)	CVPR 2023	0.895	-	-
TALL-Swin (Xu et al. 2023)	ICCV 2023	<u>0.908</u>	0.768	0.838
StyleDFD (Choi et al. 2024)	CVPR 2024	0.890	-	-
NACO (Zhang et al. 2024)	ECCV 2024	0.895	0.767	0.831
Ours	-	0.947	0.843	0.895
		($\uparrow 3.9\%$)	($\uparrow 3.9\%$)	($\uparrow 4.6\%$)

fair comparison. We also employ several widely used data augmentations, such as CutOut, and ImageCompression.

Evaluation Metrics. By default, we report the video-level Area Under the Curve (AUC) to compare our proposed method with prior works. Other evaluation metrics such as Accuracy (Acc.) and Equal Error Rate (EER) are also reported for a more comprehensive evaluation.

Evaluation Protocols. We adopt three standard protocols to evaluate our models: **Protocol-1:** cross-dataset evaluation with image methods, **Protocol-2:** cross-manipulation evaluation on the FF++ data domain, and **Protocol-3:** cross-dataset evaluation with video methods.

4.2 Protocol-1: Cross-dataset Evaluation with image detectors

In Tab. 1, we compare our method with several latest and recent SoTA detectors. Most detectors (*wo* * marker) are reproduced in our benchmark under the same settings for a fair comparison. We see that our method consistently outperforms other models across **all** tested scenarios. Note that methods with '*' do not have the complete results of all the testing datasets we used, so we leave '-' for these results.

4.3 Protocol-2: Cross-manipulation evaluation

Forgery methods in the real world can be highly diverse. Evaluating our model’s performance on cross-manipulation tasks allows us to determine whether it can handle previously unseen fake types. Instead of training and testing on the older FF++ dataset with four fake methods, we use the recently released DF40 dataset (Yan et al. 2024) for evaluation. For comparison, we select four state-of-the-art detectors, including both image and video models. Our method generally outperforms other models on average, particularly on e4s, Inswap, and SimSwap methods (see Tab. 2). This demonstrates that our method learns more general features for detection, even for the latest techniques.

4.4 Protocol-3: Cross-dataset evaluations with video detectors

Forgery methods in the real world can be highly diverse. Evaluating our model’s performance on cross-manipulation

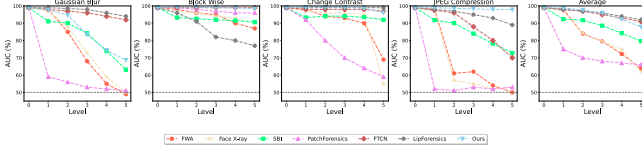


Figure 4: Robustness to Unseen Perturbations: We present video-level AUC for five distinct degradation levels across five types of perturbations in (Jiang et al. 2020).

Table 4: Ablation studies regarding the effectiveness of our proposed plug-and-play strategy (VB + StA).

Detector	#Params	Temporal	CDF-v2	DFDC	Avg.
3D-RGB (Haliassos et al. 2021)	25M	✓	0.625	0.655	0.640
3D R50 (Haliassos et al. 2021)	46M	✓	0.824	0.735	0.780
VTN (Gu et al. 2021)	46M	✓	0.734	0.691	0.713
VidTR (Zheng et al. 2021)	93M	✓	0.869	0.740	0.805
ViViT (Wang et al. 2023)	310M	✓	0.895	-	
ISTVT (Tong et al. 2022)	-	✓	0.606	0.551	0.579
ResNet-34 (He et al. 2016)	21M	✗	0.742	0.626	0.684
+ Ours	21M	✓	0.829	0.666	0.748
ViT-b16-21K (Dosovitskiy et al. 2020)	84M	✗	0.834	0.739	0.778
+ Ours	22M	✓	0.855	0.772	0.814
CLIP-b16 (Radford et al. 2021)	84M	✗	0.848	0.741	0.795
+ Ours	22M	✓	0.866	0.778	0.822
CLIP-114 (Radford et al. 2021)	307M	✗	0.900	0.798	0.854
+ Ours	46M	✓	0.947	0.843	0.895

tasks allows us to determine whether it can handle previously unseen fake types. Instead of training and testing on the older FF++ dataset with four fake methods, we use the recently released DF40 dataset (Yan et al. 2024) for evaluation. For comparison, we select four state-of-the-art detectors, including both image and video models. Our method generally outperforms other models on average, particularly on e4s, Inswap, and SimSwap methods. This demonstrates that our method learns more general features for detection.

4.5 Robustness Evaluation

To evaluate our model’s robustness to random perturbations, we adopt the methodology used in previous studies (Haliassos et al. 2021; Zheng et al. 2021), which involves examining four distinct types of degradation: Gaussian blur, Block-wise distortion, Change contrast, and JPEG compression. We apply each of these perturbations at five different levels to assess the model’s robustness under varying degrees of distortion. The video-level AUC results for these unseen perturbations, using the model trained on FF++_c23, are depicted in Fig. 4. Generally, our approach shows higher results than other methods.

4.6 Ablation Study

Effectiveness of our plug-and-play strategy. To show the *extensibility* of our method, we apply it to various architectures, including ResNet-34 (CNN) and CLIP (ViT). Results in Tab. 4 indicate that our proposed method can imbue the original model with *spatiotemporal* modeling abilities. Our method also achieves better results with fewer training parameters, emphasizing the advantages of our design.

Effectiveness of VB and StA. To evaluate the impact of the two proposed strategies (VB and StA) separately, we

Table 5: Ablation studies regarding the effectiveness of StA and VB, separately. We adopt the AUC, Acc, and EER metrics for reporting.

StA	VB	CDF-v2			WDF		
		AUC	Acc.	EER	AUC	Acc.	EER
✗	✗	0.900	0.739	0.197	0.794	0.572	0.249
✓	✗	0.926	0.812	0.195	0.842	0.654	0.222
✓	✓	0.947	0.838	0.176	0.848	0.702	0.212

Table 6: Comparison of Fixed SBI and the proposed VB.

Detector	Spatial	Temporal	CDF-v2	DFDC	Avg.
Fixed SBI (Haliassos et al. 2021)	✓	✗	0.902	0.815	0.859
VB (proposed method)	✗	✓	0.947	0.843	0.895
Fixed SBI + VB	✓	✓	0.951	0.846	0.899

conduct ablation studies on CDF-v2 and WDF. The evaluated variants include the baseline CLIP-114 without any further modifications, the baseline with the proposed StA, and our overall framework (StA + VB). The incremental enhancement in the overall generalization performance with the addition of each strategy, as evidenced by the results in Tab. 5, underscores the effectiveness of these strategies.

Image blending vs. video blending. Can image blending method, *e.g.*, SBI, act as a “video augmentor”? We designed an ablation study to investigate the effectiveness of **fixed SBI** (without temporal inconsistency) and **VB** (without spatial artifacts) in video detection. Results in Table 6 show that SBI achieves lower results than VB, but the combination of both SBI and VB is more effective than VB alone. This suggests that SBI and VB could be complementary, with one focusing on spatial aspects and the other on temporal aspects. This finding may inspire future research on how to effectively utilize both techniques to improve generalization in video detection.

5 Conclusion

In this paper, we uncover a novel and previously underexplored temporal forgery artifact present across various manipulated videos, which we term Facial Feature Drift (FFD). To simulate this artifact, we propose a novel Video-level Blending data (VB), designed to aid the model in learning more general forgery artifacts within the temporal domain. We also propose an adapter-based strategy for efficiently and effectively learning both the spatial and temporal forgery artifacts, without being overfitting to one specific type (*e.g.*, learning spatial only). Extensive experiments on several widely used and latest deepfake datasets verify the effectiveness of the proposed methods. We hope that our work will inspire further research into (1) the development of video augmentations (also the approach to combine both image and video blending), and (2) efficient spatiotemporal adapter tuning in the deepfake video detection community.

References

Cao, J.; Ma, C.; Yao, T.; Chen, S.; Ding, S.; and Yang, X. 2022. End-to-end reconstruction-classification learning for face forgery detection. In *Proceedings of the IEEE/CVF Conference on Computer Vision and Pattern Recognition*, 4113–4122.

Chen, L.; Zhang, Y.; Song, Y.; Liu, L.; and Wang, J. 2022. Self-supervised Learning of Adversarial Example: Towards Good Generalizations for Deepfake Detection. In *Proceedings of the IEEE/CVF Conference on Computer Vision and Pattern Recognition*, 18710–18719.

Cheng, J.; Zhang, Y.; Zou, Q.; Yan, Z.; Liang, C.; Wang, Z.; and Li, C. 2024. ED4: Explicit Data-level Debiasing for Deepfake Detection. *arXiv preprint arXiv:2408.06779*.

Choi, J.; Kim, T.; Jeong, Y.; Baek, S.; and Choi, J. 2024. Exploiting Style Latent Flows for Generalizing Deepfake Video Detection. In *Proceedings of the IEEE/CVF Conference on Computer Vision and Pattern Recognition*, 1133–1143.

Deepfakedetection. 2021. <https://ai.googleblog.com/2019/09/contributing-data-to-deepfakedetection.html> Accessed 2021-11-13.

Dolhansky, B.; Bitton, J.; Pflaum, B.; Lu, J.; Howes, R.; Wang, M.; and Ferrer, C. C. 2020. The deepfake detection challenge (dfdc) dataset. *arXiv preprint arXiv:2006.07397*.

Dolhansky, B.; Howes, R.; Pflaum, B.; Baram, N.; and Ferrer, C. C. 2019. The deepfake detection challenge (dfdc) preview dataset. *arXiv preprint arXiv:1910.08854*.

Dosovitskiy, A.; Beyer, L.; Kolesnikov, A.; Weissenborn, D.; Zhai, X.; Unterthiner, T.; Dehghani, M.; Minderer, M.; Heigold, G.; Gelly, S.; et al. 2020. An image is worth 16x16 words: Transformers for image recognition at scale. *arXiv preprint arXiv:2010.11929*.

Ganz, R.; Kittenplon, Y.; Aberdam, A.; Avraham, E. B.; Nuriel, O.; Mazor, S.; and Litman, R. 2024. Question Aware Vision Transformer for Multimodal Reasoning. *arXiv:2402.05472*.

Gu, Q.; Chen, S.; Yao, T.; Chen, Y.; Ding, S.; and Yi, R. 2022a. Exploiting fine-grained face forgery clues via progressive enhancement learning. In *Proceedings of the AAAI Conference on Artificial Intelligence*, 735–743.

Gu, Z.; Chen, Y.; Yao, T.; Ding, S.; Li, J.; Huang, F.; and Ma, L. 2021. Spatiotemporal inconsistency learning for deepfake video detection. In *Proceedings of the 29th ACM international conference on multimedia*, 3473–3481.

Gu, Z.; Yao, T.; Chen, Y.; Ding, S.; and Ma, L. 2022b. Hierarchical contrastive inconsistency learning for deepfake video detection. In *Proceedings of the European Conference on Computer Vision*, 596–613. Springer.

Guan, J.; Zhou, H.; Hong, Z.; Ding, E.; Wang, J.; Quan, C.; and Zhao, Y. 2022. Delving into sequential patches for deepfake detection. *Advances in Neural Information Processing Systems*, 35: 4517–4530.

Haliassos, A.; Mira, R.; Petridis, S.; and Pantic, M. 2022. Leveraging real talking faces via self-supervision for robust forgery detection. In *Proceedings of the IEEE/CVF Conference on Computer Vision and Pattern Recognition*, 14950–14962.

Haliassos, A.; Vougioukas, K.; Petridis, S.; and Pantic, M. 2021. Lips Don’t Lie: A Generalisable and Robust Approach To Face Forgery Detection. In *Proceedings of the IEEE/CVF Conference on Computer Vision and Pattern Recognition*.

He, K.; Zhang, X.; Ren, S.; and Sun, J. 2016. Deep residual learning for image recognition. In *Proceedings of the IEEE/CVF Conference on Computer Vision and Pattern Recognition*, 770–778.

Huang, B.; Wang, Z.; Yang, J.; Ai, J.; Zou, Q.; Wang, Q.; and Ye, D. 2023. Implicit Identity Driven Deepfake Face Swapping Detection. In *Proceedings of the IEEE/CVF Conference on Computer Vision and Pattern Recognition*, 4490–4499.

Jia, S.; Lyu, R.; Zhao, K.; Chen, Y.; Yan, Z.; Ju, Y.; Hu, C.; Li, X.; Wu, B.; and Lyu, S. 2024. Can chatgpt detect deepfakes? a study of using multimodal large language models for media forensics. In *Proceedings of the IEEE/CVF Conference on Computer Vision and Pattern Recognition*, 4324–4333.

Jiang, L.; Li, R.; Wu, W.; Qian, C.; and Loy, C. C. 2020. Deeperforensics-1.0: A large-scale dataset for real-world face forgery detection. In *Proceedings of the IEEE/CVF Conference on Computer Vision and Pattern Recognition*.

Kong, C.; Li, H.; and Wang, S. 2023. Enhancing general face forgery detection via vision transformer with low-rank adaptation. In *2023 IEEE 6th International Conference on Multimedia Information Processing and Retrieval*, 102–107. IEEE.

Kong, C.; Luo, A.; Bao, P.; Li, H.; Wan, R.; Zheng, Z.; Rocha, A.; and Kot, A. C. 2024a. Open-Set Deepfake Detection: A Parameter-Efficient Adaptation Method with Forgery Style Mixture. *arXiv preprint arXiv:2408.12791*.

Kong, C.; Luo, A.; Xia, S.; Yu, Y.; Li, H.; and Kot, A. C. 2024b. MoE-FFD: Mixture of Experts for Generalized and Parameter-Efficient Face Forgery Detection. *arXiv preprint arXiv:2404.08452*.

Li, L.; Bao, J.; Zhang, T.; Yang, H.; Chen, D.; Wen, F.; and Guo, B. 2020a. Face x-ray for more general face forgery detection. In *Proceedings of the IEEE/CVF Conference on Computer Vision and Pattern Recognition*.

Li, Y.; and Lyu, S. 2018. Exposing deepfake videos by detecting face warping artifacts. *arXiv preprint arXiv:1811.00656*.

Li, Y.; Yang, X.; Sun, P.; Qi, H.; and Lyu, S. 2020b. Celeb-df: A new dataset for deepfake forensics. In *Proceedings of the IEEE/CVF Conference on Computer Vision and Pattern Recognition*.

Liang, J.; Shi, H.; and Deng, W. 2022. Exploring Disentangled Content Information for Face Forgery Detection. In *Proceedings of the European Conference on Computer Vision*, 128–145. Springer.

Liu, H.; Li, X.; Zhou, W.; Chen, Y.; He, Y.; Xue, H.; Zhang, W.; and Yu, N. 2021. Spatial-phase shallow learning: re-thinking face forgery detection in frequency domain. In *Proceedings of the IEEE/CVF Conference on Computer Vision and Pattern Recognition*.

Luo, A.; Kong, C.; Huang, J.; Hu, Y.; Kang, X.; and Kot, A. C. 2023. Beyond the prior forgery knowledge: Mining critical clues for general face forgery detection. *IEEE Transactions on Information Forensics and Security*, 19: 1168–1182.

Luo, Y.; Zhang, Y.; Yan, J.; and Liu, W. 2021. Generalizing Face Forgery Detection with High-frequency Features. In *Proceedings of the IEEE/CVF Conference on Computer Vision and Pattern Recognition*.

Masi, I.; Killekar, A.; Mascarenhas, R. M.; Gurudatt, S. P.; and AbdAlmageed, W. 2020. Two-branch recurrent network for isolating deepfakes in videos. In *Proceedings of the European Conference on Computer Vision*.

Nguyen, H. H.; Yamagishi, J.; and Echizen, I. 2019. Capsule-forensics: Using Capsule Networks to Detect Forged Images and Videos. In *Proceedings of the IEEE International Conference on Acoustics, Speech, and Signal Processing*.

Ni, Y.; Meng, D.; Yu, C.; Quan, C.; Ren, D.; and Zhao, Y. 2022. CORE: Consistent Representation Learning for Face Forgery Detection. In *Proceedings of the IEEE/CVF Conference on Computer Vision and Pattern Recognition Workshop*, 12–21.

Qian, Y.; Yin, G.; Sheng, L.; Chen, Z.; and Shao, J. 2020. Thinking in frequency: Face forgery detection by mining frequency-aware clues. In *Proceedings of the European Conference on Computer Vision*.

Radford, A.; Kim, J. W.; Hallacy, C.; Ramesh, A.; Goh, G.; Agarwal, S.; Sastry, G.; Askell, A.; Mishkin, P.; Clark, J.; et al. 2021. Learning transferable visual models from natural language supervision. In *International conference on machine learning*, 8748–8763. PMLR.

Rossler, A.; Cozzolino, D.; Verdoliva, L.; Riess, C.; Thies, J.; and Nießner, M. 2019. Faceforensics++: Learning to detect manipulated facial images. In *Proceedings of the IEEE/CVF Conference on International Conference on Computer Vision*.

Shi, Y.; Gao, Y.; Lai, Y.; Wang, H.; Feng, J.; He, L.; Wan, J.; Chen, C.; Yu, Z.; and Cao, X. 2024. Shield: An evaluation benchmark for face spoofing and forgery detection with multimodal large language models. *arXiv preprint arXiv:2402.04178*.

Shiohara, K.; and Yamasaki, T. 2022. Detecting deepfakes with self-blended images. In *Proceedings of the IEEE/CVF Conference on Computer Vision and Pattern Recognition*, 18720–18729.

Sun, K.; Liu, H.; Yao, T.; Sun, X.; Chen, S.; Ding, S.; and Ji, R. 2022a. An information theoretic approach for attention-driven face forgery detection. In *European Conference on Computer Vision*, 111–127. Springer.

Sun, K.; Yao, T.; Chen, S.; Ding, S.; Li, J.; and Ji, R. 2022b. Dual contrastive learning for general face forgery detection. In *Proceedings of the AAAI Conference on Artificial Intelligence*, volume 36, 2316–2324.

Tong, Z.; Song, Y.; Wang, J.; and Wang, L. 2022. Video-mae: Masked autoencoders are data-efficient learners for self-supervised video pre-training. *Advances in neural information processing systems*, 35: 10078–10093.

Wang, C.; and Deng, W. 2021. Representative Forgery Mining for Fake Face Detection. In *Proceedings of the IEEE/CVF Conference on Computer Vision and Pattern Recognition*.

Wang, Z.; Bao, J.; Zhou, W.; Wang, W.; and Li, H. 2023. AltFreezing for More General Video Face Forgery Detection. In *Proceedings of the IEEE/CVF Conference on Computer Vision and Pattern Recognition*, 4129–4138.

Xu, Y.; Liang, J.; Jia, G.; Yang, Z.; Zhang, Y.; and He, R. 2023. Tall: Thumbnail layout for deepfake video detection. In *Proceedings of the IEEE/CVF International Conference on Computer Vision*, 22658–22668.

Yan, Z.; Luo, Y.; Lyu, S.; Liu, Q.; and Wu, B. 2023a. Transcending forgery specificity with latent space augmentation for generalizable deepfake detection. *arXiv preprint arXiv:2311.11278*.

Yan, Z.; Sun, P.; Lang, Y.; Du, S.; Zhang, S.; Wang, W.; and Liu, L. 2022. Multimodal Graph Learning for Deepfake Detection. *arXiv preprint arXiv:2209.05419*.

Yan, Z.; Yao, T.; Chen, S.; Zhao, Y.; Fu, X.; Zhu, J.; Luo, D.; Yuan, L.; Wang, C.; Ding, S.; et al. 2024. DF40: Toward Next-Generation Deepfake Detection. *arXiv preprint arXiv:2406.13495*.

Yan, Z.; Zhang, Y.; Fan, Y.; and Wu, B. 2023b. UCF: Uncovering Common Features for Generalizable Deepfake Detection. *arXiv preprint arXiv:2304.13949*.

Yan, Z.; Zhang, Y.; Yuan, X.; Lyu, S.; and Wu, B. 2023c. DeepfakeBench: A Comprehensive Benchmark of Deepfake Detection. *arXiv preprint arXiv:2307.01426*.

Yang, X.; Li, Y.; and Lyu, S. 2019. Exposing Deep Fakes Using Inconsistent Head Poses. In *Proceedings of the IEEE International Conference on Acoustics, Speech, and Signal Processing*.

Zhang, D.; Xiao, Z.; Li, S.; Lin, F.; Li, J.; and Ge, S. 2024. Learning Natural Consistency Representation for Face Forgery Video Detection. *arXiv preprint arXiv:2407.10550*.

Zheng, Y.; Bao, J.; Chen, D.; Zeng, M.; and Wen, F. 2021. Exploring Temporal Coherence for More General Video Face Forgery Detection. In *Proceedings of the IEEE/CVF Conference on International Conference on Computer Vision*, 15044–15054.

Zhou, P.; Han, X.; Morariu, V. I.; and Davis, L. S. 2017. Two-Stream Neural Networks for Tampered Face Detection. In *Proceedings of the IEEE/CVF Conference on Computer Vision and Pattern Recognition Workshop*.

Zhou, T.; Wang, W.; Liang, Z.; and Shen, J. 2021. Face forensics in the wild. In *Proceedings of the IEEE/CVF Conference on Computer Vision and Pattern Recognition*, 5778–5788.

Zhu, X.; Wang, H.; Fei, H.; Lei, Z.; and Li, S. Z. 2021. Face forgery detection by 3d decomposition. In *Proceedings of the IEEE/CVF Conference on Computer Vision and Pattern Recognition*, 2929–2939.

Zhuang, W.; Chu, Q.; Tan, Z.; Liu, Q.; Yuan, H.; Miao, C.; Luo, Z.; and Yu, N. 2022. UIA-ViT: Unsupervised inconsistency-aware method based on vision transformer for face forgery detection. In *Proceedings of European Conference on Computer Vision*, 391–407. Springer.

Zi, B.; Chang, M.; Chen, J.; Ma, X.; and Jiang, Y.-G. 2020. Wilddeepfake: A challenging real-world dataset for deepfake detection. In *Proceedings of the 28th ACM international conference on multimedia*, 2382–2390.